Wetting Topology in Trickle Bed Reactors

Loïc Baussaron, Carine Julcour-Lebigue, Anne-Marie Wilhelm, and Henri Delmas
Laboratoire de Génie Chimique de Toulouse, 5 rue Paulin Talabot BP 1301, 31106 Toulouse Cedex 1, France

Christophe Boyer
Institut Français du Pétrole, IFP-Lyon, BP3, 69390 Vernaison, France

Local and average partial wetting efficiencies in trickle-beds have been directly measured by image processing and PIV analysis. Two different setups have been implemented: a vertical monolayer of pellets where the wetting structure and stability and also local velocity gradient are characterized by PIV, and a fixed bed to analyze (by photography) the axial evolution of wetting over bed cross section after a transient injection of dye. Porous alumina spheres and different liquids have been used to examine the effect of liquid–solid affinity; two liquid distributors, and bed prewetting were investigated at low liquid superficial velocities (0.5×10^{-3}–10^{-2} m/s). Contrary to usual techniques (excepting MRI), not only average wetting efficiencies are derived from the colorimetric tracing, but also local features: axial evolution of wetting, size, and locations of dry zones, distributions of wetting efficiency at a particle scale. All those local data are important to improve reactor models assuming uniform pellet wetting. The effect of liquid–solid affinity is predominant in the case of the monolayer of beads, and, contrary to usual assumption, is still significant for the real trickle bed in the low range of wetting efficiency, corresponding to liquid superficial velocity lower than 2×10^{-3} m/s. © 2007 American Institute of Chemical Engineers AIChE J, 53: 1850–1860, 2007
Keywords: wetting efficiency, trickle-bed reactor, PIV, image processing, dye-adsorption, wettability, contact angle

Introduction

Trickle-bed reactors are packed beds of catalyst particles with cocurrent downflow of liquid and gas reactants. Their use is widespread in petroleum industry particularly in hydrotreatment processes such as hydrodesulfurization and hydrocracking. Bench-scale reactors usually operate at the same liquid hourly space velocities as the commercial reactors, leading to very low liquid velocities and partial wetting

of the catalyst. Partial wetting can result in a poor utilization of the catalyst and in hot spots formation.

According to the value of the gas and liquid flow rates encountered in both industrial and pilot plants, liquid flows over the solid in the form of films, rivulets or droplets: this flow texture has been investigated by Charpentier et al.[1,2] These authors showed that the liquid flow on the packing of absorption columns was heterogeneous with isotropic structures as films, and anisotropic ones as rivulets and drops. In trickle-bed reactors films, quasi-stagnant pockets of liquid and rivulets may exist, but probably no drops. But very few results can be found on the effect of static wettability, quantifying the affinity between the solid and the liquid, on
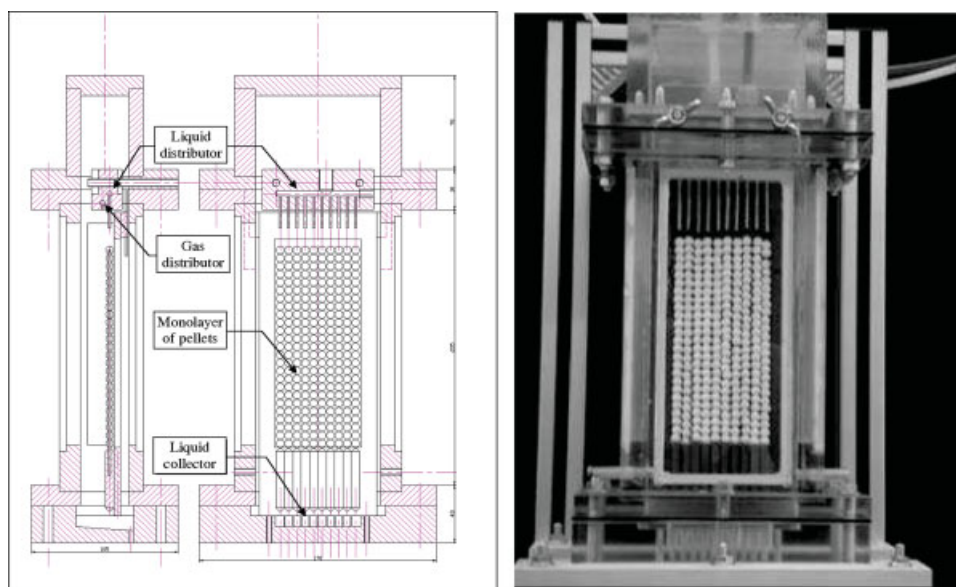
Figure 1. Bidimensional monolayer of pellets.

[Color figure can be viewed in the online issue, which is available at www.interscience.wiley.com.]

the wetting efficiency f in fixed-bed, that is, the fraction of the catalyst external surface, which is wetted by flowing liquid. Ortiz-Arroyo et al.[3] showed theoretically, by solving the equation of Young–Laplace on two identical spheres in contact on a vertical line, that the contact angle had an important influence on the meniscus, which is formed between the two particles. Khanna and Nigam[4] developed a conceptual approach for a better understanding of the relation between wettability and wetting efficiency on a porous support. Contrary to the intuition, they considered that wetting efficiency does not increase regularly with wettability. The authors highlight an improving effect of solid particles porosity on the spreading out of the liquid. They confirmed this effect with a perforated plate modeling a porous substrate and showed that internal wetting improves external wetting by the formation of liquid bridges. The pores of catalyst also drive the liquid rivulets, which flow from pores to pores.[5] Let us notice however that the "pores" of these experiments are holes of several millimeters, very far from the usual size of catalyst pores.

But no studies are able to discriminate the effects of physicochemistry and hydrodynamics on the spreading out of the liquid in the case of a complex geometry, as a bed of particles.

However, several methods have been proposed to measure the wetting efficiency f in trickle-bed reactors: dynamic tracer technique,[6,7] chemical reaction method,[8] and more recently, hydrodynamic technique[9] and magnetic resonance imaging technique (MRI).[10] Except MRI, all those approaches are overall, indirect, and require a model of reactor involving hydrodynamic, transfer, and/or kinetic parameters.

Ravindra et al.[11] proposed a dye-adsorption technique to investigate qualitatively features of liquid flow texture inside a trickle bed at different depths. They completed these bed-scale visualizations by measuring exit liquid distributions and pressure drop.

Very recently, van Houwelingen et al.[12] used a similar technique to derive wetting efficiencies for different modes of prewetting.

When investigating catalyst wetting in a trickle-bed reactor, the question always arises about how the liquid is locally distributed inside the bed: is a pellet-scale wetting or a bed-scale wetting to be considered, what is the evolution of the dry/wetted features along the bed height?

For simplicity and as usual measuring techniques give only an overall value of the wetting efficiency, usual reactor models assume that all pellets are equally wetted whatever the gas and liquid flow rates, the liquid distribution, or the prewetting.

In this study, two methods have been developed to directly measure wetting efficiencies to understand qualitative trends, but also to quantify particle-scale wetting, distributions of wetting in a column, as well as liquid film velocities. These techniques allow to answer the previous questions and to quantify the extent of error when assuming a uniform wetting.

These two methods are based on image processing and PIV analysis of a colored tracer injected in the liquid phase, and are carried out in two different setups:

• a bidimensional monolayer of pellets where the liquid phase is seeded with micronic rhodamine/PMMA particles illuminated by an expanded laser beam,

• a fixed bed consisting of two concentric columns, where the inner one is coupled to a piston, able to push the bed upward once the experiment is completed and to unload the bed by 11 sections to investigate the axial evolution of wetting after circulating a liquid dye solution through the bed.

The use of porous alumina spheres and different liquids (ethanol, water, heptane) allowed to investigate the effect of liquid–solid affinity on the wetting efficiency.

During this study, the effects of liquid distribution and of the bed prewetting were first investigated. Then, a local study was carried out to determine a wetting efficiency per pellet,
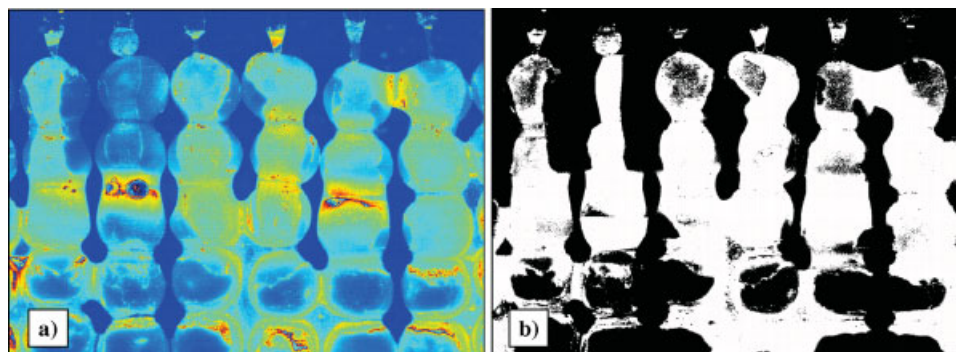
Figure 2. (a) Rough image of the flow and (b) binary image of the flow.

[Color figure can be viewed in the online issue, which is available at www.interscience.wiley.com.]

a distribution of wetting efficiency in a column cross-section, and a characteristic scale of dry zones. Finally, the effect of physicochemistry was put forward on the average wetting efficiency of the column.

Experimental

Two-dimensional monolayer of pellets

Description of the Setup. A schematic diagram of the two-dimensional monolayer is presented in Figure 1. Pellets of 6×10^{-3} m in diameter are pierced along a diameter and stringed on 10 vertical metal stems fixed at the top and bottom so that to avoid any contact between the transparent PVC back-wall of the setup and the particles. The liquid distributor is a tube connected to 10 needles, which distribute the liquid uniformly on each row of pellets. The distributor can be moved (from left to right and from back to front) to sprinkle the axis of the beads or their periphery. The liquid flow rate, measured by a Coriolis mass flow-meter, ranges between 1.4×10^{-7} and 1.4×10^{-6} m^3/s ("superficial" linear velocities from 0.4×10^{-3} to 4×10^{-3} m/s were calculated by dividing the flow rate by the area of the rectangular cross-section of the flow: one pellet diameter versus 10 pellets diameters) and allows to cover a broad range of wetting efficiencies.

Measuring Technique. The PIV system, provided by LaVision Company, involves a camera recording images of seed particles illuminated by a front laser beam at successive instants. The liquid phase is seeded with fluorescent particles (rhodamine/PPMA) of diameters ranging between 1 and 20 μm, sufficiently large to be visible with the camera, but small enough to enable the flow through the needles. The laser source used is a pulsed laser delivering two pulses of several tens of millijoules, the time interval being adjustable according to the range of liquid velocities. The front of the setup is illuminated by the laser and this illuminated zone is relatively broad, 0.03–0.04 m on each side. The magnitude of the depth of focus is one particle radius, contrary to the traditional PIV, which uses a fine laser sheet perpendicular to the camera. The movement of the particles is recorded by a CCD camera (12 bits, 1376×1040 pixels resolution). Rhodamine re-emitting the laser light at a known wavelength (580 nm), an interferential filter centered on the rhodamine wavelength allowed to get rid of reflections and re-emission by the beads. A record involves 30 couples of images and lasts $\sim$10 s.

The wetting efficiency is calculated after processing the rough images, and the velocity fields were evaluated to differentiate the stagnant and dynamic zones.

Image Processing. Various treatments, carried out on Matlab, were applied to the rough images of flow (Figure 2a: water-alumina) to calculate the wetting efficiency f.

The first step consisted of traditional image processing:

• binarization (Figure 2b) to determine the liquid fraction represented in white,

• multiplication by the binarized blank image (image without flow showing the solid fraction, Figure 3a) to keep only the fraction of liquid on the pellets,

• morphological operation (closing) to make continuous the wet zones (Figure 3b). This morphological operation is essential for a good evaluation of the wet zones, which
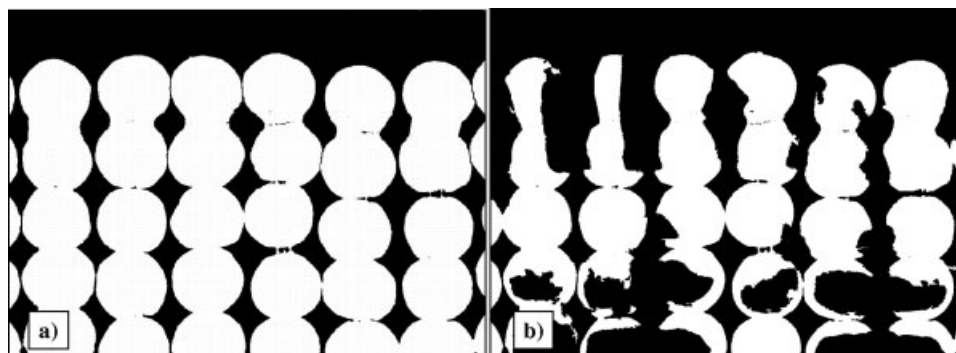
Figure 3. (a) Binary image of the layer without flow and (b) image of the flow after morphological treatment.
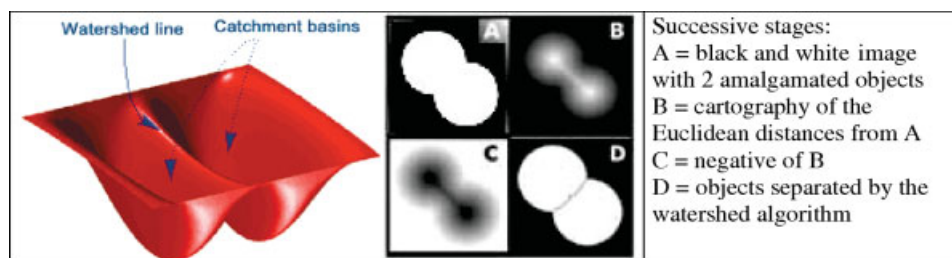
Figure 4. Segmentation of objects in a black and white image by the watershed transform ("watershed line").[13]

[Color figure can be viewed in the online issue, which is available at www.interscience.wiley.com.]

appear "discontinuous," because of detection of the rhodamine particles present in the liquid on the beads.

Each step was performed using existing functions of the Image Processing toolbox from Matlab.

The second step of the image treatment was to take account of the sphericity of the alumina particles. The real surface of the half-spheres is rebuilt (Figure 5) from the surface projected on the 2D image by multiplying the surface of successive crowns by its "weight" $\alpha_{k(i,j)}$, increasing from the center to the outside of the pellet. $\alpha_{k(i,j)}$ is calculated as the ratio between the real surface of the crown and its projected surface. The 3D image of the dry bed (accessible to the camera) is thus completely rebuilt. This method of rebuilding, which must be carried out sphere by sphere, was validated by calculating the surface of a half-sphere starting from a disc of known diameter. With 30 crowns, the difference between the rebuilt surface and the real surface is only 2%.

A semiautomatic treatment for the recognition of objects was also developed to extract each particle as a separate object and measure its 3D wetted fraction. The first step of this procedure consists in segmenting the particles on the black and white image as illustrated in Figure 4. A chart of the Euclidean distances from the complementary image is carried out to differentiate in levels of gray the successive zones from the center towards the periphery of the objects. The objects are then separated by the "watershed algorithm." The second step is the detection of the objects and the comparison with discs filling the square in which the object is inscribed (Matlab function by John McCarthy). Each disc is then divided into crowns to form the 2D/3D mask of projection, which is initially multiplied by the basic image without flow (Figure 3a) to be used as reference (3D image without flow). Then, the binarized image with flow (on pellets only,

Figure 3b) is multiplied by this 3D/2D mask as presented in Figure 5. The "true" wetting efficiency (*f*) is finally calculated by dividing the wet surfaces area by the solid surface of the particle; the wet surface is the sum of $\alpha_{k(i,j)}$. $P_{i,j}$ of the 3D image with flow ($P_{i,j}$ being equal to 1 if the pixel *i,j* is filled with liquid and to 0 elsewhere), and the solid surface is given by the sum of the $\alpha_{k(i,j)}$. $P'_{i,j}$ of the 3D image without flow ($P'_{i,j}$ being equal to 1 if the pixel *i,j* is filled with solid and to 0 elsewhere).

$$f = \frac{\sum (P_{i,j})_{\text{image withflow}} \alpha_{k(i,j),\, \text{mask 3D/2D}}}{\sum (P'_{i,j})_{\text{image withoutflow}} \alpha_{k(i,j),\, \text{mask 3D/2D}}}$$
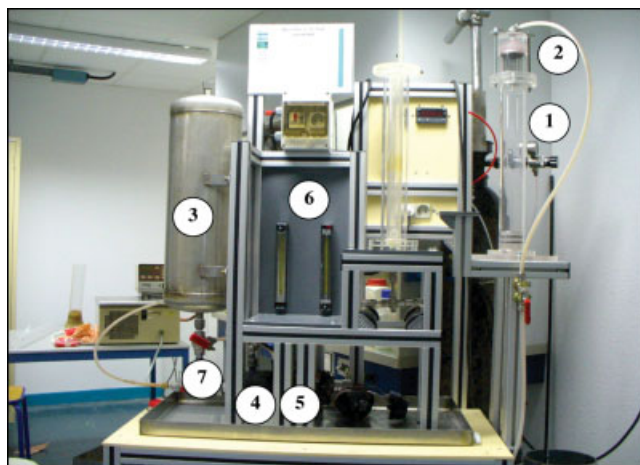
The fixed bed for dye-adsorption

Description of the Setup. The second setup, used for the dye adsorption tests, is presented in Figures 6 and 7. Two tanks respectively contain pure liquid (3) and colored liquid (3′). A three-way valve (7) makes it possible to rock quickly from one feed to the other. The liquid, moved by a gear pump, is introduced at the top of the column and distributed independently of the gas. The geometry of the distributor (Figure 7b), involving 49 capillaries of 10^{-3} m internal diameter and 0.1 m length (9), allows a good distribution of the liquid and of the gas on the column cross-section. A space hollowed in an altuglas part (8) ensures a minimum level of liquid above the capillaries to homogenize its distribution. The gas, supplied by a cylinder, is injected into the intermediate space of the distributor (10) and is distributed, independently of the liquid, by 24 openings of 2×10^{-3} m in diameter (11). The column consists in two concentric tubes, the inner one being divided into 11 slices, 0.035 m in
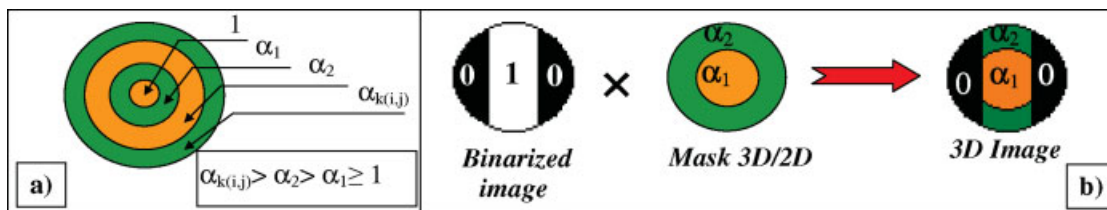
Figure 5. 3D treatments.

(a) The pellet projection is divided in successive crowns: 1, 2, . . . , *k*. (b) The contribution of each pixel of coordinates (*i,j*) is weighted (factor $\alpha_k(i,j)$) according to its location in one of these crowns (i.e., the 3D area it represents). [Color figure can be viewed in the online issue, which is available at www.interscience.wiley.com.]

Figure 6. Photograph of the fixed bed reactor for dye-adsorption.

(1) Column, (2) gas–liquid distributor, (3) liquid storage tank, (4) gear pump, (5) Coriolis mass flow meter, (6) gas flow meters, and (7) three-way valve. [Color figure can be viewed in the online issue, which is available at www.interscience.wiley.com.]

height and 0.057 m in internal diameter, which allow the investigation of the axial evolution of wetting efficiencies.

A piston is placed at the bottom of the column. At the end of the test, the fixed bed can thus be pushed upwards and cut slice by slice to determine the axial evolution of the wetting efficiency by image analysis. The loading of the bed was carried out according to a precise protocol. A 0.5 m length sleeve is added at the top of column to ensure a sufficient falling speed to the particles. The amount of loaded particles is weighed for each test to check the reproducibility of the fixed bed voidage.

Measuring Techniques. The colorimetric tracing is used to chart the bed. The bed is flooded with single liquid flow during 5 min, drained and then it is fed with gas and pure liquid during 30 min to make sure that steady state is reached. The three-way valve is then commutated for the colored liquid injection. The dyes used are eosin in water and ethanol, Sudan red in heptane. The concentrations were selected to obtain an important contrast between the wet and dry zones, without modifying γ_L. The colored liquid circulates during 5–30 min, according to the studied flow-rate, then the supply of tracer is cut off and a step of rinsing with pure liquid is carried out. The bed is drained, the distributor is withdrawn, and the plate for the particles collection installed. The hinged jib supporting the camera (13) is placed at the top of the bed and the taking of photographs of bed cross section is carried out. The piston is pushed upwards and the first section of tube withdrawn, the pellets contained in the section are evacuated and a new photograph is taken. A second series of photos is obtained by spreading out a sample of the pellets contained in each slice on a perforated plate to get wetting efficiency following random orientations.

For this method, the time duration of the dye solution injection is optimized so that all active zones of the bed can be irrigated by the solution without any color spreading across the particle by diffusion.

Image Processing. The image processing associated to the colorimetric measurements is slightly different from the one developed previously. Figure 8 presents an example of photographs (Figure 8a) and of the treatment applied (Figures 8b–d).

First, the processed area is defined by locating a circle on the rough image, and removing at the column wall the equivalent of a diameter of particles so that the edge of the column does not appear on the treated image.

Then, the image is divided into three zones: wet zones (in red on the Figure 8b), dry zones (in white on the Figure 8c), and interparticle spaces of dark color for which no distinction can be made between wet and dry. The algorithm $a \times b \times L$ of the toolbox Image Processing of Matlab makes it possible to separate these three colors thanks to two criteria: the levels of color a (from red to green) and b (from blue to yellow), and the luminosity L. The luminosity is necessary to differentiate black and white when the only criterion of color does not allow it. For each color, a group of pixels is selected on the image and for each area, the values of a, b, and L are calculated.

The colored markers of each zone have thus an identified value of a, b, and L for each processed image. They are used to classify each pixel by calculating the Euclidean distance between the pixel and each marker:

• The pixel is initially regarded as "red" or "not red" according to the Euclidean distance to the markers, calculated with the two criteria of color, a and b.

• For the zones, which are regarded as not red, according to the criterion of luminosity, the pixel is viewed as "white" or "black."

At the end of this first treatment, an average value of the wetting efficiency on the section can be calculated as the surface ratio of the red zones to the sum of the white and red zones.
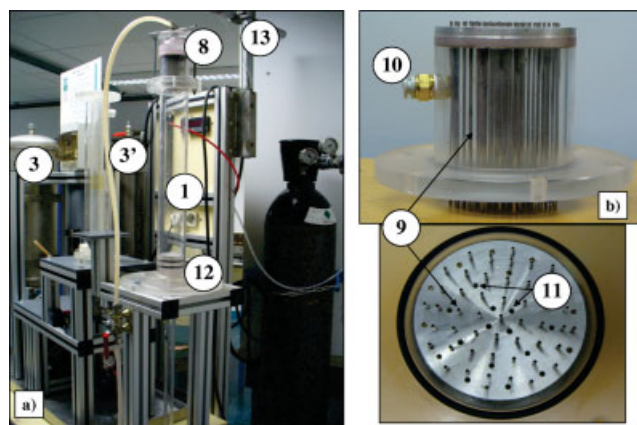
Figure 7. (a) Fixed bed reactor and (b) gas–liquid distributor for dye-adsorption.

(1) Column, (3 and 3′) liquid storage tanks (pure/colored), (8) hollowed headspace of the distributor, (9) capillaries, (10) gas inlet, (11) gas distributor, (12) piston to move the inner column, and (13) hinged jib supporting the camera. [Color figure can be viewed in the online issue, which is available at www.interscience.wiley.com.]
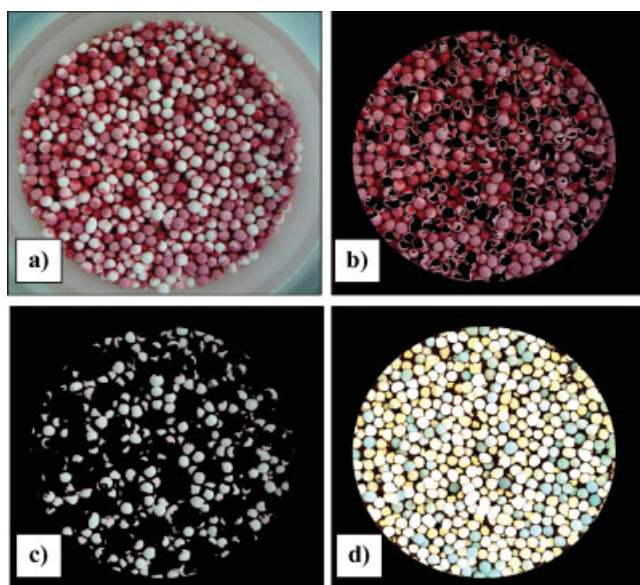
Figure 8. (a) Rough image (b) wet zones, (c) dry zones, and (d) segmentation result.

[Color figure can be viewed in the online issue, which is available at www.interscience.wiley.com.]

The second step separates the objects (Figure 8d) thanks to a recognition software and an automatic differentiation, based on the watershed algorithm (as described previously).

These "section views" obtained along the column by taking photographs of the cross-section on the top of each module are very useful to locate some typical flow structures (large dry zones or regular patterns of liquid distribution) and thus to chart the bed axially. These pictures have two drawbacks: they are taken from the top of the column and only show the top half of the beads (facing the flow) and they characterize only a 2D cross-section and not a 3D volume of bed. Therefore "volume views" were carried out by taking a representative sample of the pellets included in the slice volume and spreading it randomly on a perforated plate. Average wetting efficiencies were calculated for a section volume, and the wetting efficiency per particle could be estimated, independently of the orientation of the particle in the bed.

Table 1. Operating Conditions and Properties of the Two Phases

Studied Parameters	Range
Liquid	
Nature	Water, heptane, ethanol
ρ_L, kg m^{-3}	700–1000
μ_L, Pa s	$0.4 \times 10^{-3} - 1.1 \times 10^{-3}$
V_{LS}, m s^{-1}	$0.2 \times 10^{-3} - 10^{-2}$
Catalyst pellet	
Shape	Sphere
Nature	Alumina
d_p, m	$2.5 \times 10^{-3}, 6 \times 10^{-3}$
Pressure, Pa	Atmospheric
Temperature, K	298

Table 2. Physical Properties of the Solid Particles

	d_p, m	ρ_s, kg/m^3	ε_i	a_s, m^2/g
Pellet A	6×10^{-3}	2886	0.517	277
Pellet B	2.5×10^{-3}	3804	0.75	192
Pellet C	2.5×10^{-3}	3195	0.591	83

Operating conditions

The operating conditions ranges are summarized in Table 1 for the two experimental setups. Three liquids and several sizes of alumina particles are studied. The tests are carried out at ambient temperature and atmospheric pressure, with no gas flow.

Various types of alumina, with different structural densities, internal porosities ε_i, and specific areas have been used for these experiments (Table 2). Two particles diameters were studied, 2.5×10^{-3} and 6×10^{-3} m in diameter.

Results and Discussion

Monolayer of pellets

Effects of the Liquid Flow Rate and Liquid–Solid Affinity. Two qualitative observations could be noticed concerning the film flow structure over the pellet surface:

• The position of the rivulets proved to be very stable, which validates the dye-adsorption method that integrates the wetting history in the final result.

• If the liquid distribution is intermittent (drop by drop), the liquid front moves along the particles surface in the form of drops or of film with "waves," according to the feed frequency (the time-evolution of the wetting efficiency is periodic).

Then, Figure 9 shows the evolution of the wetting efficiency with the liquid flow rate: f increases in a very moderate way with liquid flow rate. This result is in agreement with the literature where the wetting efficiency increases moderately with the liquid flow rate, generally as $Q_L{}^\beta$ with $0.1 < \beta < 0.4$.[7,14] Our experimental results are compared with the correlations of El-Hisnawi[15] and Burghardt[16] for water flow over porous particles and appear consistent with Burghardt's correlation results.
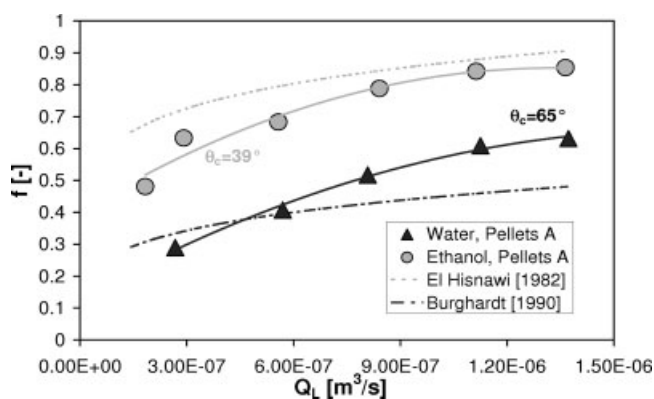
Figure 9. Evolution of wetting efficiency with liquid flow rate (f is calculated on a 6 × 6 pellets zone at the middle of the layer).
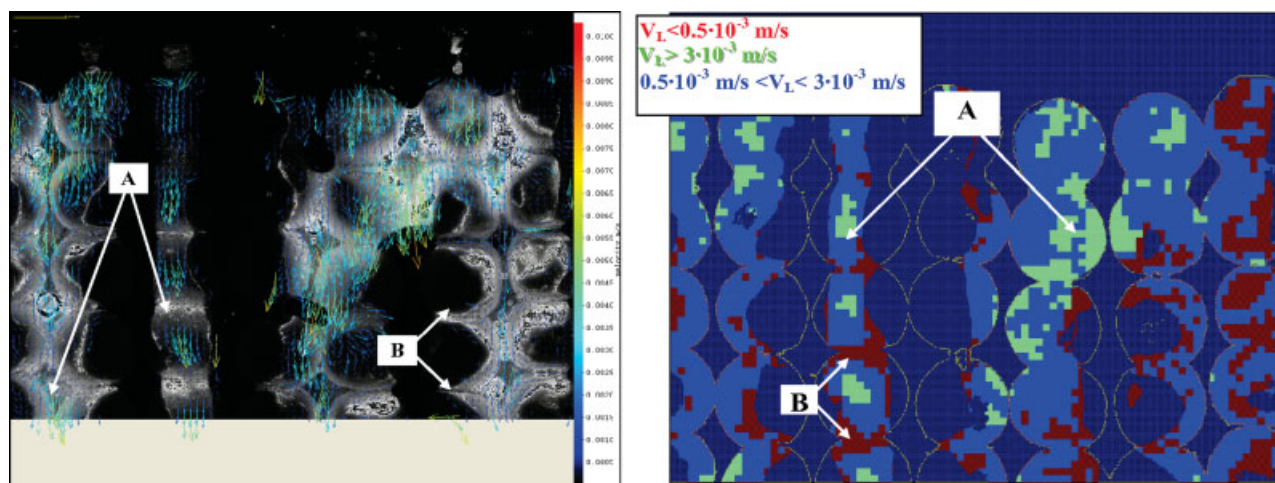
Figure 10. Velocity field (water-pellets A; $Q_L = 1.4 \times 10^{-6}$ m^3/s): (a) velocity vectors, (b) chart of velocity vectors modules.

[Color figure can be viewed in the online issue, which is available at www.interscience.wiley.com.]

Liquid–solid affinity has been quantified by the contact angle, θ_c, measured by the Washburn method, based on the dynamics of the capillary impregnation of a dry fixed bed of particles in contact with a static liquid. Liquid–solid affinity seems a key factor on the wetting efficiency. For the pellets A, the wetting efficiency increases by 30–50% when changing from water (liquid–solid contact angle $\theta_c = 65°$) to ethanol ($\theta_c = 39°$). Wetting efficiency appears to be strongly dependent on liquid/solid affinity variations. Indeed, when the contact angle increases, the liquid flows in thicker but narrower films, which results in a decrease of the wetting efficiency.

Dynamics of the Flow. The velocity fields were estimated with PIV measurements only for the water-alumina system. It can be noticed that there are strong velocities gradients between the center and the edge of the liquid vein. Figure 10a shows that there is no completely motionless liquid.

In Figure 10b, a chart of the velocity vectors modules is proposed, revealing three zones (when considering only the liquid flowing on the particles) according to their color:

Red: $V_L < 0.5 \times 10^{-3}$ m/s (zone B), light blue: 0.5×10^{-3} m/s $< V_L < 3 \times 10^{-3}$ m/s, green: 3×10^{-3} m/s $< V_L$ (zone A).

Table 3 shows that liquid flow rate has only very little effect on the distribution of these velocity zones. In all cases, the velocities between the rows of particles and on the surface of particles (zone A, 3×10^{-3} to 5×10^{-3} m/s) are 10–20 times higher than at the contact points between two spheres placed one at the top of the other or on the frontline dry-wet zones (zone B, 0 to 0.5×10^{-3} m/s).

• In zone B, which account for 15–20% of total wetting efficiency (Figure 10b, in red), the film tends to thicken because of liquid accumulation.

• In zone A, there is an acceleration of the liquid film with reduction of the film thickness.

The stability of these percentages of slow and fast liquid with liquid flow rates suggests that the difference between these flows comes mainly from the interstitial liquid. The streaming flow thus proceeds by very important accelerations and decelerations between the quasi-stagnant zones localized at the poles of the particles.

Trickle bed setup

Figure 11 is an example of a photograph taken in the column (section-view). It can be noticed that the borders between the dry and wet zones are very clear.

Effect of Prewetting. Experiments were carried out with and without bed prewetting to investigate the influence of the start-up procedure on the wetting efficiency. Prewetting consists in filling the column with only liquid, the exit valve being closed and the liquid flow rate being very low to avoid the trapping of air bubbles. Then the liquid is flushed out before the beginning of the trickling flow. Photographs presented Figure 12 ($V_{LS} = 2 \times 10^{-3}$ m/s) illustrate the clear effect of prewetting. Indeed, two large dry zones appear along the bed axis when no prewetting is performed. As shown in Figure 12c, the dry zones can disappear from an axial position to another, in particular for high liquid velocities.

The values of the wetting efficiency calculated from the Figure 12 images confirm the qualitative results obtained from image analysis and the large effect of prewetting on the average wetting efficiency (Figure 13a), especially at low liquid flow rates. Without prewetting, the average wetting effi-

Table 3. Proportions of Stagnant and Dynamic Liquid on the Pellets

|	$Q_L = 2.8 \times 10^{-7}$ m^3 s^{-1}, $V_{LS} = 0.8 \times 10^{-3}$ m s^{-1}	$Q_L = 1.4 \times 10^{-6}$ m^3 s^{-1}, $V_{LS} = 4 \times 10^{-3}$ m s^{-1}
Slow liquid zone B ($V_L < 0.5 \times 10^{-3}$ m/s)	18%	19%
Fast liquid zone A ($V_L > 3 \times 10^{-3}$ m/s)	13%	15%

Figure 11. Picture of a column cross-section (pellets A; $V_{LS} = 2 \times 10^{-3}$ m/s; water).

[Color figure can be viewed in the online issue, which is available at www.interscience.wiley.com.]

ciency is at least 10% lower than the value obtained with prewetting, and this difference increases when liquid velocity decreases. At low liquid velocities, completely dry zones are formed in the absence of prewetting due to severe channel flow, which will limit the performances of the reactor. This channeling is important as long as the liquid flow is not high enough to force new paths inside the bed.

As alumina particles are porous, liquid fills the pores under the effect of the capillary forces during the bed prewetting. Then, bridges are formed between intra and extra particle liquid and facilitate the spreading out of films on the particle by surface tension effect, *liquid attracting liquid*. These conclusions join those presented by Maiti et al.[5] These authors used a tilting perforated plate to represent a porous particle. They highlighted that the liquid drops in contact with "the pores" of the particle filled by liquid required a higher gravity force effect (i.e., a higher inclination angle of the plate) to be taken down.

The absence of prewetting makes the space distribution of the liquid very random and also probably nonreproducible. Indeed, the average wetting efficiency for $V_{LS} = 10^{-3}$ m/s is slightly higher than for $V_{LS} = 2 \times 10^{-3}$ m/s because of the
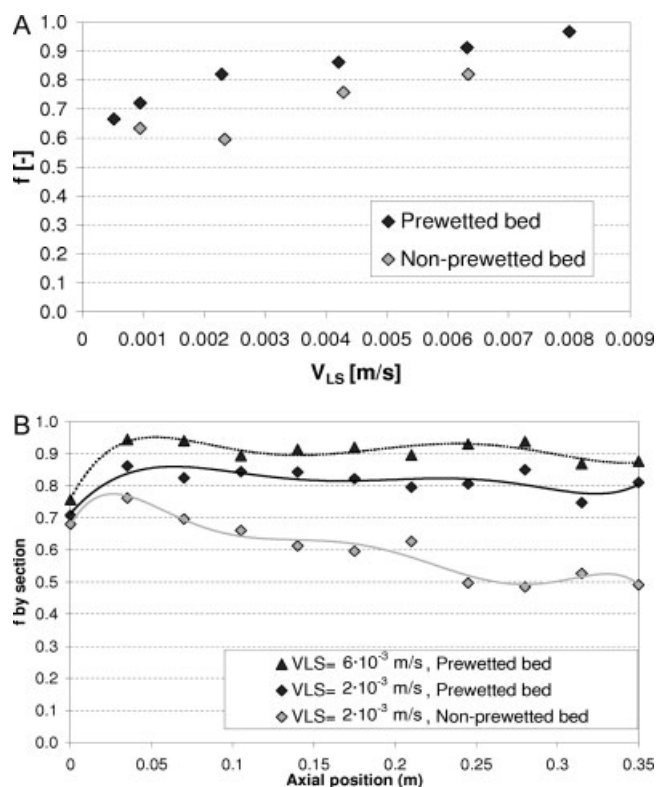
Figure 13. (a) Effect of prewetting (pellets C; heptane): effect on the average wetting efficiency; (b) effect of prewetting (pellets C; heptane): axial evolution of wetting efficiency.

presence of the two dry zones at $V_{LS} = 2 \times 10^{-3}$ m/s (Figure 12b). Without prewetting, the liquid distribution appears to be mainly influenced by the packing local properties.
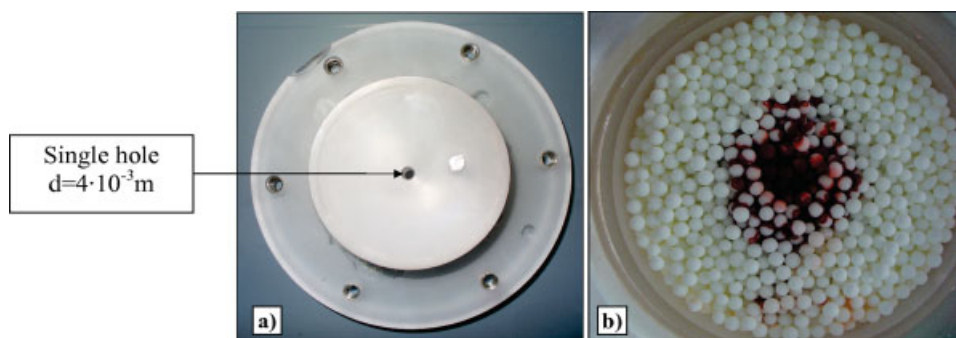
On the other hand, bed prewetting assures a good reproducibility of the wetting efficiencies.
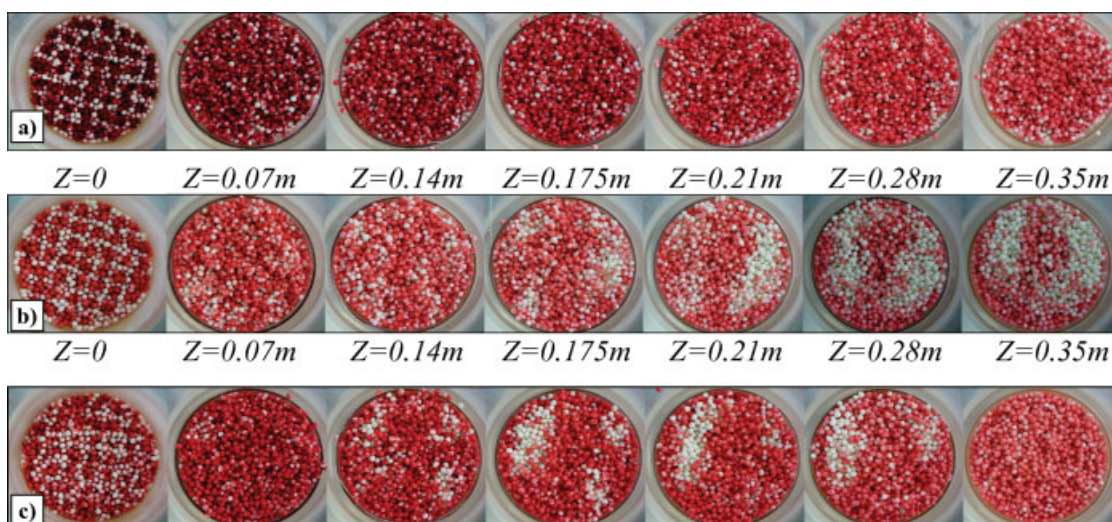
Figure 12. Axial evolution of wetting efficiency (pellets C; heptane): (a) prewetted bed: $V_{LS} = 2 \times 10^{-3}$ m/s; (b) non-prewetted bed: $V_{LS} = 2 \times 10^{-3}$ m/s; (c) nonprewetted bed: $V_{LS} = 6 \times 10^{-3}$ m/s.

[Color figure can be viewed in the online issue, which is available at www.interscience.wiley.com.]

Figure 14. (a) Monocapillary distributor; (b) distribution at the bed inlet ($Z = 0$).

Figure 13b presents the axial evolution of the wetting efficiency with and without prewetting. When the bed is prewetted, the length needed for the wetting efficiency to be established lies between 0.03 and 0.05 m for $V_{LS} > 2 \times 10^{-3}$ m/s (i.e., ~15 particle diameters). For very low liquid flow rates, this axial establishment length can be a little longer. On the other hand, without prewetting, 0.2 m are necessary to get stable cross sectional averaged values of f (for $V_{LS} = 2 \times 10^{-3}$ m/s)

To conclude this study, prewetting has been confirmed

• to yield a homogeneous liquid distribution on the cross-section of the reactor within a lower distance,

• to allow more reproducible wetting structures,

• to get average higher wetting efficiencies (of about 10%) than without prewetting.

Effect of Liquid Distribution. The influence of the distributor on the wetting efficiency has been evaluated by comparing a monocapillary distributor (Figure 14a), provided with a single central hole of 4×10^{-3} m in diameter located on the reactor axis, to the multicapillary one (described in experimental section). In Figure 14b, a "cross-section view" at $Z = 0$ demonstrates the point distribution induced by the single point distributor, the irrigated zone accounting for only 25% of the cross-section.

Figure 15 presents the evolution of average wetting efficiency in the column with the superficial liquid velocity, for the prewetted pellets B and the two distributors: monocapillary and multicapillary.

For $V_{LS} > 2 \times 10^{-3}$ m/s, the average wetting efficiency is similar for both distribution modes (difference less than 5%). The fixed bed compensates for the very poor distribution because of the monocapillary distributor and allows a homogeneous distribution on the bottom of the reactor. On the other hand, the difference between the two modes of injection increases when $V_{LS} = 2 \times 10^{-3}$ m/s, to become very large at 10^{-3} and 0.5×10^{-3} m/s, the liquid flow concentrating in the axial part of the reactor. The variation on f can reach 40% and very broad dry zone appear in the column.

A homogeneous distribution of the liquid flow at the top of the column guarantees a still better liquid distribution in the reactor and reduces the radial heterogeneities of wetting efficiency, even at low superficial liquid velocity.

Size and Locations of the Dry Zones. For a prewetted bed with the multicapillary distributor, the evolution of the size and the position of the dry regions has been investigated

($V_{LS} = 2 \times 10^{-3}$ m/s and 6×10^{-3} m/s). The cross-section of the column is divided into two zones (Figure 16) of same area: the central and the surrounding zones. Then, the surface area and the position of the gravity centre of each dry structure have been determined, and the surface area is compared to the area of one particle (2.5×10^{-3} m in diameter for pellets B). A histogram is plotted where the dry structures are classified by their surface areas (in particles numbers), and differentiated along with the location of their gravity center (in the central or surrounding zone). This stacked column chart presents the ratio of area of these dry structures on the overall dry projected surface (in percents) and their size in X-coordinate.

Figure 17 presents the axial evolution of the size and the position of these dry structures. Two superficial liquid velocities are studied: 6×10^{-3} and 2×10^{-3} m/s, leading to average wetting efficiencies of ~0.8 and ~0.55, respectively.

For these two velocities, the largely majority class is that of the small structures: smaller than one pellet. These dry zones are very homogeneously distributed between the center and the periphery of the column. Moreover, almost no axial evolution was observed. Nevertheless, the largest structures (obtained at low velocity), equivalent to 10 particles, are met near the wall of the column rather than in the central zone of the bed.

Wetting Efficiency Distribution. Figure 18 presents the distribution of wetting efficiency at a particle scale for two
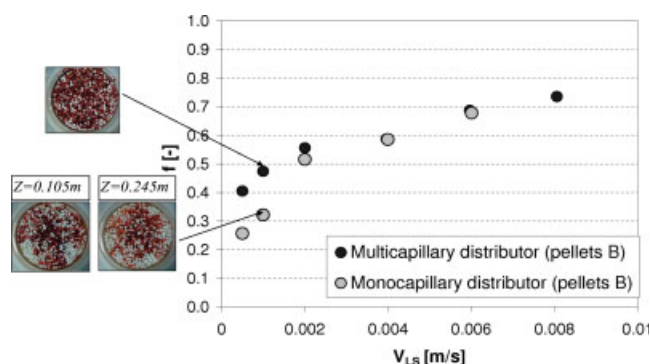
Figure 15. Evolution of the average wetting efficiency with liquid velocity for the two injectors (prewetted pellets B; heptane).
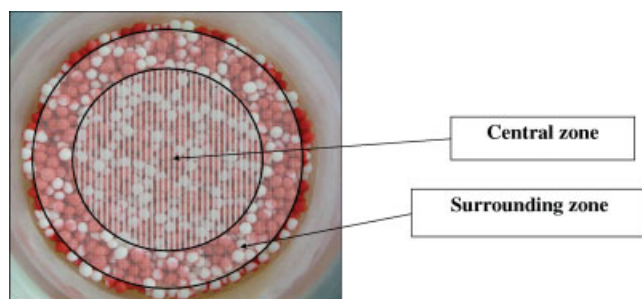
Figure 16. Position of the central zone and surrounding zones of the cross-section.

[Color figure can be viewed in the online issue, which is available at www.interscience.wiley.com.]

Figure 18. Wetting efficiency distribution for two different liquid velocities (pellets B; heptane).

values of V_{LS}. In both cases, the majority classes are the extreme ones and a minimum appears at an intermediate class. At $V_{LS} = 8 \times 10^{-3}$ m/s, for a total wetting efficiency of 0.75, ~45% of pellets are almost completely wet, the other classes gathering only 5–10% of particles. When superficial liquid velocity decreases, the fraction of pellets in the intermediate classes is not as strongly modified as in the extreme classes (dry and totally wetted particles). This is due to a balance in between the adjacent classes, which do not occur for extreme classes. For the lowest velocity ($V_{LS} =$
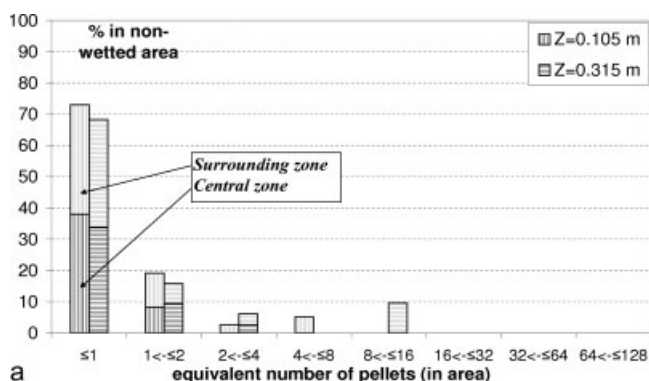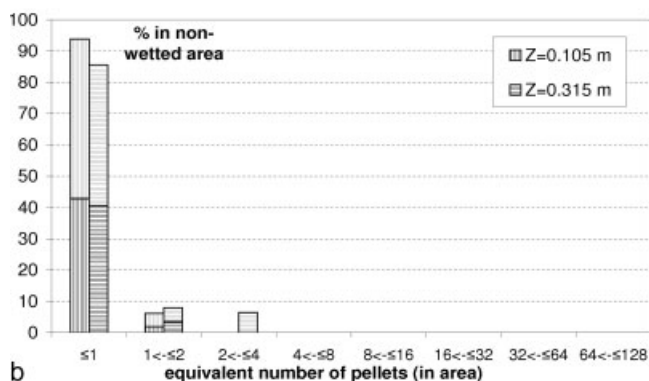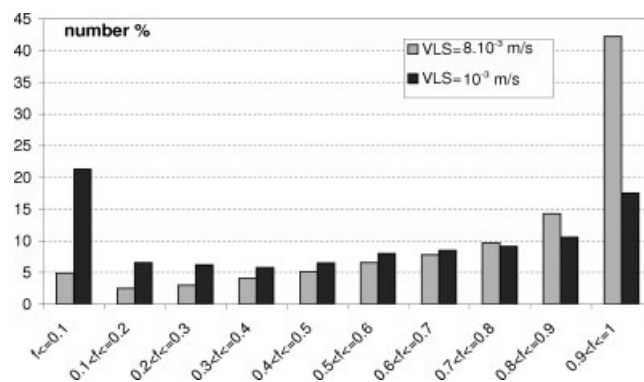

Figure 17. (a) Axial evolution of the size and position of the nonwetted structures (pellets B; heptane): $V_{LS} = 2 \times 10^{-3}$ m/s; (b) Axial evolution of the size and position of the nonwetted structures (pellets B; heptane): $V_{LS} = 6 \times 10^{-3}$ m/s.

10^{-3} m/s), only 18% of the particles are completely wet whereas nearly 20% of the pellets are almost dry.

Effect of Liquid–Solid Affinity on Wetting Efficiency. The results obtained on the two-dimensional setup proved that the nature of the phases held a key-role on the wetting efficiency. Therefore, the average wetting efficiency in the trickle bed column was measured for different liquids: water, ethanol, and heptane. Figure 19 presents the evolution of the wetting efficiency with the liquid velocity for these three liquids. These liquids have very different affinities for alumina. The contact angles measured by the Washburn technique are 65°, 39° for water, and ethanol, respectively, and 0° for heptane since it has been selected as the reference totally wetting liquid for the Washburn method.

The smaller the contact angle is, the stronger the affinity of the liquid for the solid is, and the thinner and wider the liquid film.

However, for $V_{LS} > 2 \times 10^{-3}$ m/s, Figure 19 shows that the wetting efficiencies measured with heptane are only 5% higher than those measured with water. Indeed, contrary to monolayer configuration, because of bed confinement, the liquid holdup is increased inducing a high number of bridges between liquid films, and the effect of the liquid–solid affinity is erased. On the other hand, at low liquid velocities, the difference in wetting efficiencies for the two fluids is more significant, up to 30% for $V_{LS} = 0.5 \times 10^{-3}$ m/s. For this velocity, the amount of liquid is not sufficient to cover the
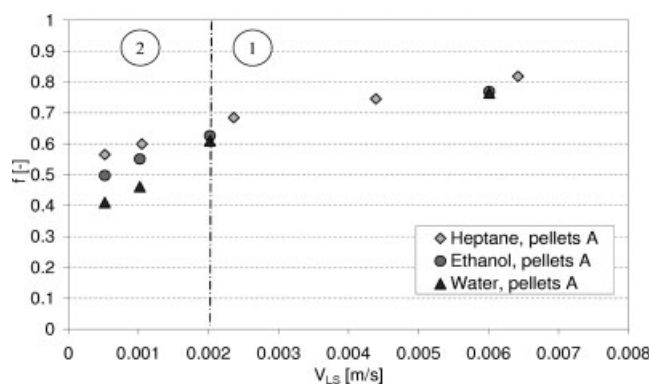
Figure 19. Effect of liquid–solid affinity on average wetting efficiency.

major part of the particles and the liquid–solid affinity is the key-factor for the geometry of the liquid film. For a wetting liquid, the film is less thick and wider, the wetting efficiency is thus higher. In addition, the less wetting the liquid is, the larger the impact of V_{LS} is at these low V_{LS} values.

To conclude, two operating zones are thus to distinguish, based on liquid superficial velocity range:

• in zone 1 ($V_{LS} > 2 \times 10^{-3}$ m/s), the wetting efficiency is mainly conditioned by hydrodynamics,

• in zone 2 ($V_{LS} < 2 \times 10^{-3}$ m/s), liquid–solid affinity controls wetting efficiency f. These results moderate the results obtained on the bidimensional setup.

This set of data of averaged wetting efficiency has been completed and used to develop a new correlation for wetting efficiency prediction, including not only the effect of hydrodynamics, but also that of physicochemistry (through capillary numbers based on gas/liquid and liquid/solid surface tensions).[17]

Conclusion

Different setups, experimental methods, and image processing have been implemented and validated to detect wetting structures inside a catalytic bed exposed to a gas–liquid trickling flow. The results obtained put forward the great interest of these direct techniques of image acquisition and processing for the direct measurement of local wetting efficiencies.

The local study, carried out in a bidimensional monolayer of pellets, yielded a direct access to the dynamic wetting efficiency, highlighting the dominating effect played by liquid–solid affinity. A second study, carried out in a real trickle bed with dye-adsorption method, showed that in a correctly prewetted bed and so far as the liquid phase is homogeneously distributed, there is no structuring of the local wetting: the characteristic size of dry zones is not larger than one particle diameter. In these conditions, it is fully justified to consider a pellet-scale wetting when modeling a trickle-bed reactor with a homogeneous liquid distribution, but it is more controversial to assume that all pellets are equally wetted when only 15–30% of the particles exhibit a wetting efficiency equal to the mean value within ±20% range.

This is no more the case in a nonprewetted bed, where large dry zones are created over the entire length of the bed.

The effects of liquid–solid affinity observed on the local model were a little bit moderated by the results of the trickle bed: the very important containment, which exists in a stacking of particles in a real bed improves liquid film damping and reduces the effect of liquid–solid affinity for $V_{LS} > 2 \times 10^{-3}$ m/s. On the other hand, for low liquid velocity, wettability always controls the wetting efficiency and should be accounted for in its modeling.

Notation

a_s = BET surface area, m^2/g.
d_p = particle diameter, m.
f = external wetting efficiency.
$P_{i,j}$ = value of each pixel i,j in the binarized image.
Q_L = liquid flow rate, m^3/s.
V_L = local liquid velocity, m/s.
V_{LS} = superficial liquid velocity, m/s.

Greek letters

$\alpha_{k(i,j)}$ = ratio of the real and projected surface areas for a crown.
γ_L = liquid surface tension, N/m.
ε_i = internal porosity.
θ_c = three-phase contact angle, deg.
μ_L = dynamic liquid viscosity, Pa s.
ρ_L = liquid density, kg m^{-3}.
ρ_S = structural solid density, kg m^{-3}.

Literature Cited

1. Charpentier JC, Prost C, van Swaaij W, Le Goff P. Etude de la rétention de liquide dans une colonne à garnissage arrosé à co-courant et à contre-courant de gaz-liquide. Représentation de sa texture par un modèle à films, filets et gouttes. *Chim Ind Génie Chim*. 1968;99:803–826.
2. Charpentier JC, Prost C, Le Goff P. Ecoulement ruisselant de liquide dans une colonne à garnissage. Détermination des vitesses et des débits relatifs des films, des filets et des gouttes. *Chim Ind Génie Chim*. 1968;100:653–665.
3. Ortiz-Arroyo A, Larachi F, Iliuta I. Method for inferring contact angle and for correlating static liquid hold-up in packed beds. *Chem Eng Sci*. 2003;58:2835–2855.
4. Khanna R, Nigam KDP. Partial wetting in porous catalysts: wettability and wetting efficiency. *Chem Eng Sci*. 2002;57:3401–3405.
5. Maiti RN, Arora R, Khanna R, Sen PK, Nigam KDP. The liquid spreading on porous solids: dual action of pores. *Chem Eng Sci*. 2005;60:6235–6239.
6. Colombo AJ, Baldi G, Sicardi S. Solid-liquid contacting effectiveness in trickle bed reactors. *Chem Eng Sci*. 1976;31:1101–1108.
7. Al-Dahhan MH, Dudukovic MP. Catalyst wetting efficiency in trickle-bed reactors at high pressure. *Chem Eng Sci*. 1995;50:2377–2389.
8. Llano JJ, Rosal R, Sastre H, Diez FV. Determination of wetting efficiency in trickle-bed reactors by a reaction method. *Ind Eng Chem Res*. 1997;36:2616–2625.
9. Pironti F, Mizrahi D, Acosta A, Gonzalez-Mendizabal D. Liquid-solid wetting factor in trickle bed reactors: its determination by a physical method. *Chem Eng Sci*. 1999;54:3793–3800.
10. Gladden LF, Mantle MD, Sederman AJ, Yuen EHL. Magnetic resonance imaging of single and two-phase flow in fixed-bed reactors. *Appl Magn Reson*. 2002;22:201–212.
11. Ravindra PV, Rao DP, Rao MS. Liquid flow texture in trickle-bed reactors: an experimental study. *Ind Eng Chem Res*. 1997;36:5133–5145.
12. van Houwelingen AJ, Sandrock C, Nicol W. Particle wetting distribution in trickle-bed reactors. *AIChE J*. 2006;52:3532–3541.
13. Eddins S. The watershed transform—strategies for image segmentation. *Newsletters—MATLAB News & Notes*, February 2002.
14. Ring ZE, Missen RW. Trickle-bed reactors: tracer study of liquid holdup and wetting efficiency at high temperature and pressure. *Can J Chem Eng*. 1991;69:1016–1020.
15. El-Hisnawi AA, Dudukovic MP, Mills PL. Trickle-bed reactors: dynamic tracer tests, reaction studies, and modeling of reactor performance. *ACS Symp Ser*. 1982;196:421–440.
16. Burghardt A, Kolodziej AS, Jaroszynski M. Experimental studies of liquid-solid wetting efficiency in trickle-bed cocurrent reactors. *Chem Eng Process*. 1990;28:35–49.
17. Baussaron L. Etude du mouillage partiel et du transfert de matière liquide-solide en réacteur à lit fixe arrosé. Ph.D. Thesis, INP Toulouse (France), 2005. Available at http://ethesis.inp-toulouse.fr/archive/00000249/01/baussaron.pdf.